Available online at www.sciencedirect.com
SCIENCE DIRECT®
International Journal of Mass Spectrometry 241 (2005) 139–147
International Journal of Mass Spectrometry
www.elsevier.com/locate/ijms

Polyatomicity and kinetic energy effects on surface polymerization by ion-assisted deposition

Yongsoo Choi, Adam Zachary, Sanja Tepavcevic, Chunping Wu, Luke Hanley*

Department of Chemistry (m/c 111), University of Illinois at Chicago, Chicago, IL 60607-7061, USA

Received 8 November 2004; accepted 15 December 2004

Abstract

Various techniques are used to probe surface polymerization by ion-assisted deposition (SPIAD) of films prepared from 100 and 200 eV non-mass-selected thiophene ions and evaporated α-terthiophene (3T) neutrals. $C_4H_4S^+$, $C_4D_4S^+$ (and fragments thereof), and Ar^+ ions are compared to elucidate polymerization mechanisms in SPIAD. Desorption ionization on oxidized silicon mass spectrometry is used to probe the nature of the polymerized products of SPIAD as well as ion incorporation into the film. Mass spectra, Fourier transform infrared spectra, and X-ray diffraction all indicate higher molecular weight species and less fragmentation of 3T for 100 eV thiophene ions. Mass spectra indicate thiophene ions behave both as catalysts and reagents in polymerization. Despite obvious differences in film chemistry, quartz crystal microbalance measurements show SPIAD film thicknesses are the same for both the polyatomic and atomic ions at both ion energies. UV–vis absorption and photoluminescence are found to depend upon the differing chemical composition and structure of the films which in turn are controlled by the polyatomicity and kinetic energy of the incident ions.

Keywords: Surface polymerization; Polythiophene; Ion deposition; Ion-assisted deposition; Desorption ionization on oxidized silicon

1. Introduction

Conducting polymers are currently being considered for use in various thin film devices including field effect transistors, light emitting diodes, and photovoltaics [1]. Optimization of thin film devices requires an ability to fine tune optoelectronic properties via modification of film chemical and morphological structure. Control of optical band gaps and emission in such films has been most commonly achieved through electrochemical and chemical synthesis methods [2,3], but there is strong interest in other methods that allow improved in situ control and modification of film properties. Ion-assisted deposition is one method previously shown to allow control of optoelectronic properties of organic films [4–8].

Previous work showed that polymerization of evaporated α-terthiophene (3T) or *p*-terphenyl films can be efficiently promoted by the simultaneous impact of hyperthermal polyatomic thiophene ions onto a surface [9,10]. This method is termed surface polymerization by ion-assisted deposition (SPIAD) and it allows growth of conducting polymer films with control over their UV–vis absorption and photoluminescence spectra which depend upon both ion energy and ion to neutral ratio [11]. While film growth rates are similar at different ion energies, mass spectra indicate the formation of different distributions of polymerized species. However, further study of the mechanism of film polymerization and control of optical properties in SPIAD is warranted.

The present paper examines the overall effect of incident ion polyatomicity and kinetic energy on the polymerization and optical properties of the polythiophene which here is termed a SPIAD film. The question addressed is whether it matters if polyatomic ions are used in SPIAD or if the same films are produced by atomic ions. Previous reports examined

* Corresponding author. Tel.: +1 3129960945; fax: +1 3129960431.
E-mail address: LHanley@uic.edu (L. Hanley).

1387-3806/$ – see front matter © 2004 Elsevier B.V. All rights reserved.
doi:10.1016/j.ijms.2004.12.022

the effect of ions – either polyatomic [7,8] or atomic [4,6] – on the optical or optoelectronic properties of organic films formed by ion-assisted deposition. These reports showed that both polyatomic and atomic ions induce significant changes in optical or optoelectronic properties of films compared to their evaporated film counterparts. Modification was generally related to film structure and an efficient hole/electron recombination mechanism, but many relevant issues were not discussed including the specific role of film chemical structure, the extent of polymerization of the neutral monomer, and the potential incorporation of the ion into the film. Various mechanistic issues in SPIAD are addressed in the present paper through the use of a separate source of ions and neutrals. Both 100 and 200 eV energy polyatomic ions – non-mass-selected thiophene ions – and Ar^+ atomic ions are compared for 3T SPIAD film growth. Mass spectra of films prepared by hydrogenated and deuterated thiophene ions probe ion incorporation into the film. UV–vis absorption and photoluminescence probe optical properties and a quartz crystal microbalance compares film thicknesses. Crystalline structures of the 3T SPIAD films grown by thiophene ions versus Ar^+ are examined by X-ray diffraction. These results are discussed in terms of polymerization mechanisms and the relationship of optical properties to film structure.

2. Experimental details

2.1. Film deposition conditions and substrate

SPIAD films are created by co-depositing thermal α-terthiophene neutrals (3T or 2,2′:5,2′-terthiophene, 98%, Alfa Aesar) and non-mass-selected Ar^+ or thiophene ions onto a substrate surface. Deposition is performed onto various substrates, depending upon the analysis method (as described individually below). The experimental conditions and apparatus which include the ion source, mass flow controller, and energy analyzer/quadruple mass spectrometer were described previously [11]. Briefly, a commercial Kaufman ion source using 30 eV electron impact energy (Model 3 cm Ion Source, Veeco-CS) generates Ar^+ or thiophene ions from a precursor gas metered by a mass flow controller (Type 246, MKS). Monitoring ion fragmentation by an energy analyzer/quadrupole mass spectrometer finds that ∼65% of the ions formed from thiophene gas in this source are the intact thiophene parent ion, $C_4H_4S^+$, with the remainder fragments thereof. An 8 μA/cm^2 ion current and a 45° incident ion angle are used for all film depositions except for those onto the quartz crystal microbalance (QCM), which utilizes a 2 μA/cm^2 ion current. All SPIAD films are grown at 1/100 ion to neutral flux ratio. A bias of −40 eV is applied to the substrate to achieve 100 eV kinetic energy for deposition at the desired ion current. No bias voltage is applied to the substrate during deposition of 200 eV kinetic energy ions which is achieved instead by increasing the beam voltage by variation of potentials in the ion source. 3T is thermally evaporated onto the substrate in vacuum using a resistively heated doser (Model LTE 11000K, 1 cc, Kurt J. Lesker) and the neutral flux is monitored by a QCM (Model SQC-222, Sigma Instruments). The neutral flux calculation from the QCM frequency shift was described previously [11]. Total ion and neutral fluxes used for the SPIAD films are $\sim 4 \times 10^{16}$ cm^{-2} and $\sim 7 \times 10^{18}$ cm^{-2}, respectively, except as noted below.

The QCM is most conveniently employed by multiple depositions onto the same Au coated crystal that is sputter cleaned between each deposition. Beams of ∼50 μA, 350 eV Ar^+ ions are used to sputter each deposited film until the initial QCM frequency is recovered, thereby avoiding frequency dependent errors in the QCM measurement. A 1 cm^2 electrically insulated metal plate is installed in front of the QCM shutter to measure the ion current. Total ion and neutral fluxes used for the QCM measurements are $\sim 4 \times 10^{15}$ cm^{-2} and $\sim 8 \times 10^{17}$ cm^{-2}, respectively. Films deposited on the QCM are subsequently heated in vacuum with an infrared lamp for 1800 s, then stored in vacuum for an additional 3600 s to ensure complete sublimation of all unbounded 3T, all the while monitoring the QCM frequency. Film thicknesses are obtained from the QCM frequency changes through calibration based upon thicknesses from cross sections of thicker films measured by variable pressure scanning electron microscopy (Model S3000N VPSEM, Hitachi, 5 keV electron beam voltage, no film coating). It is found that film thicknesses from electron microscopy of 1.5 ± 0.03 μm (∼9× thicker than the other deposited films described herein) correspond to a QCM frequency shift of 9080 ± 25 Hz.

2.2. Characterization of film optical properties

Photoluminescence (PL) at 390 nm excitation wavelength of the films is measured with the same instrument (SLM Aminco 8000C, ISS) under previously described conditions [11]. UV–vis absorption is measured using a standard instrument (Model Cary 100 & 300 series, Varian) equipped with a solid sample holder and sample masking area of 1 cm^2. SPIAD films for optical measurements are deposited onto indium tin oxide (ITO) coated glass substrates.

2.3. Characterization of film chemistry and crystallinity

Commercially available desorption ionization on oxidized silicon (DIOS) chips were used previously to characterize films in a matrix-assisted laser desorption ionization reflectron time-of-flight mass spectrometer (Model Voyager-DE PRO 6275, Applied Biosystems) [11,12]. The work described here requires investigation of larger film areas than those probed using the commercially available DIOS chips, so similar chips are fabricated in house. The electrochemical fabrication process involves connecting a p-doped silicon wafer in HF acid (24 wt.% in ethanol) to the anode of an electrolytic power supply and oxidizing into a 0.7 cm^2 effective area at ∼20 mA for 300 s under white light illumination from an in-

candescent bulb [13]. Mass spectra of 100 eV films directly deposited onto these homemade DIOS chips are identical to those of films deposited onto commercial DIOS chips.

Fourier transform infrared (FTIR) absorption of films deposited onto Si wafers is performed within the vacuum chamber (Model FTLA 2000-154, Bomem ABB) with an optical path that includes the vacuum chamber and a narrow band MCT detector. Infrared radiation from the FTIR passes through the film and Si substrates at normal angle and spectra are recorded with 350 scans at 4 cm^{-1} resolution. A hydrogen-terminated surface is prepared on the Si substrate prior to SPIAD by first etching with 5% HF solution for 40 s, then by rinsing with deionized water to remove the native SiO_2 layer [11].

The crystalline structure of the films is analyzed by X-ray diffraction (XRD) using a standard powder diffractometer utilizing θ–2θ scans (Model D-5000, Siemens, Cu Kα X-rays). Films analyzed by XRD are deposited onto hydrogen-terminated Si substrates, but the films are approximately twice as thick as those grown for the other characterization methods to allow improved S/N. Total ion and neutral fluxes used for the XRD measurements are $\sim 7 \times 10^{16}\,cm^{-2}$ and $\sim 1.5 \times 10^{18}\,cm^{-2}$, respectively. The XRD measured films are also kept in vacuum at room temperature for at least 24 h before XRD scanning, to allow full evaporation of unbound 3T.

3. Results

3.1. Optical properties from UV–vis absorption and photoluminescence

Fig. 1 shows 390 nm excited photoluminescence (PL) for evaporated α-terthiophene (3T) films and SPIAD films produced by either thiophene and its fragment ions (T^+ SPIAD) or argon ions (Ar^+ SPIAD) deposited at 100 and 200 eV kinetic energy coincident with 3T evaporation. PL of T^+ SPIAD at 100 and 200 eV energy (1/100 ion to neutral ratio) was investigated previously [11] and displayed a red shift with two new peaks at 535 and 570 nm. Both ions at 100 eV kinetic energy induce the strongest enhancement in PL intensity for SPIAD films compared with the 3T evaporated film while the 200 eV ion energy leads to dramatically reduced PL intensity. The PL of Ar^+ SPIAD films at 100 and 200 eV are similar to those of T^+ SPIAD in that they shift to the red compared to the 3T evaporated film PL. However, there are several differences in PL for the atomic versus polyatomic ions. The T^+ SPIAD film PL displays its most intense peak at 535 nm with lesser peak shoulders at 505 and 550 nm. The Ar^+ SPIAD PL displays its most intense peak at 505 nm and a second most intense peak at 550 nm.

Fig. 2 shows the UV–vis absorption of the 3T evaporated, T^+ SPIAD, and Ar^+ SPIAD films deposited at 100 eV. The center of the absorption peak of the 3T evaporated film occurs at 320 nm, while it is shifted to 350 nm for the Ar^+ SPIAD film and 370 nm for the T^+ SPIAD film. There is also a broad tail in the absorption ranging from 420 to ~550 nm for the Ar^+ SPIAD film which extends further to ~660 nm for the T^+ SPIAD film. This tail is absent in the UV–vis absorption of the 3T evaporated film, which cuts off sharply at 420 nm.

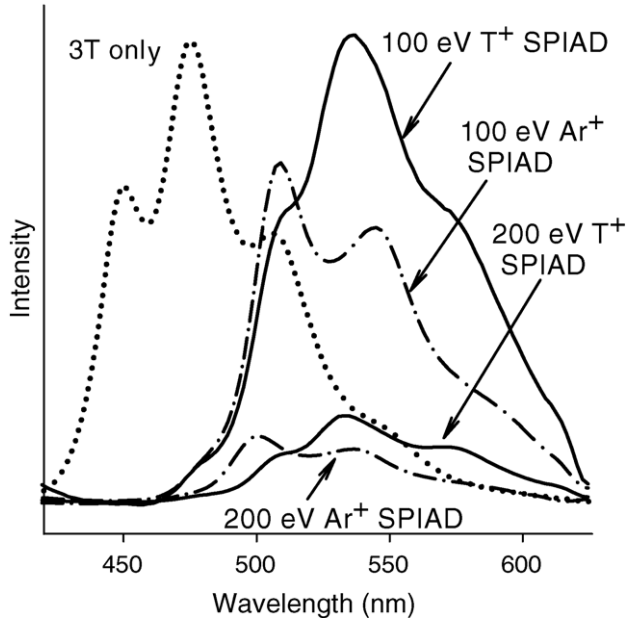

Fig. 1. Photoluminescence (PL) of evaporated α-terthiophene (3T) films as well as thiophene ion (T^+) surface polymerization by ion-assisted deposition (SPIAD) and Ar^+ SPIAD films grown at 100 and 200 eV ion energies (1/100 ion to 3T neutral ratios). Films are grown on indium tin oxide coated (ITO) glass and PL are measured at 390 nm excitation. T^+ refers to $C_4H_4S^+$ and fragments thereof.

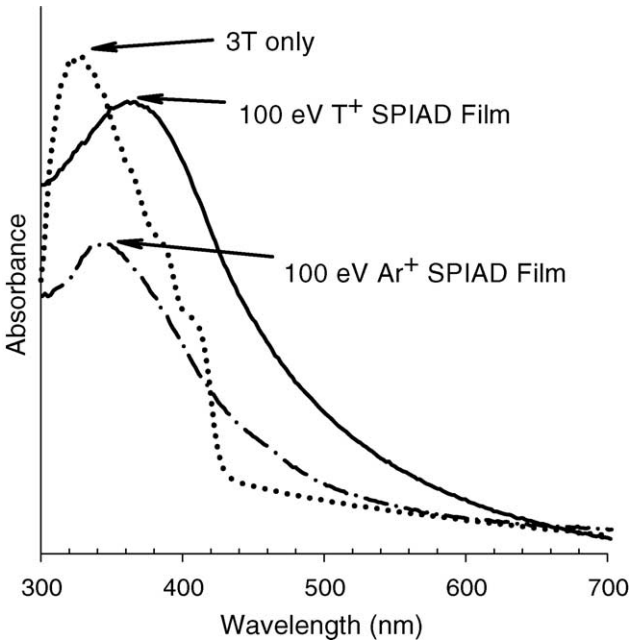

Fig. 2. UV–vis absorption of evaporated 3T, 100 eV T^+ SPIAD, and 100 eV Ar^+ SPIAD films on ITO glass.

3.2. Deposition, sublimation, and overall thicknesses from QCM

Direct thiophene ion deposition (without any 3T evaporation), T^+ SPIAD, and Ar^+ SPIAD films at both 100 and 200 eV are investigated by following the frequency change of a quartz crystal microbalance (QCM), as shown in Fig. 3. The QCM frequency does not change for the first 420 s prior to deposition, but the frequency dramatically decreases during the 420 s of ion and 3T neutral deposition. Turning off the ion and neutral sources at the end of deposition and turning on an infrared lamp located inside the vacuum chamber causes a sharp increase in frequency as the deposited film is heated and unbound 3T sublimes. The largest frequency change in the SPIAD film deposition is completed after ~2000 s in vacuum, indicating that 3T sublimation is mostly complete. However, a slower frequency change continues for another ~1500 s. No large dip in the frequency is observed for the direct ion deposition experiments, as there is no 3T to sublime (see inset of Fig. 3).

The net change in frequency from deposition is measured 3600 s after the start of deposition, as shown in the inset of Fig. 3. A net frequency change is observed only for SPIAD and direct ion deposited films while 3T evaporated films completely sublime and induce no net frequency change (data not shown), as expected. Fig. 4 shows the thickness of direct ion deposited, T^+ SPIAD, and Ar^+ SPIAD films produced by 100 and 200 eV ions. Film thicknesses from the QCM are shown in Fig. 4 and range from 155 to 170 nm for all SPIAD films within error, regardless of ion energy and ion structure

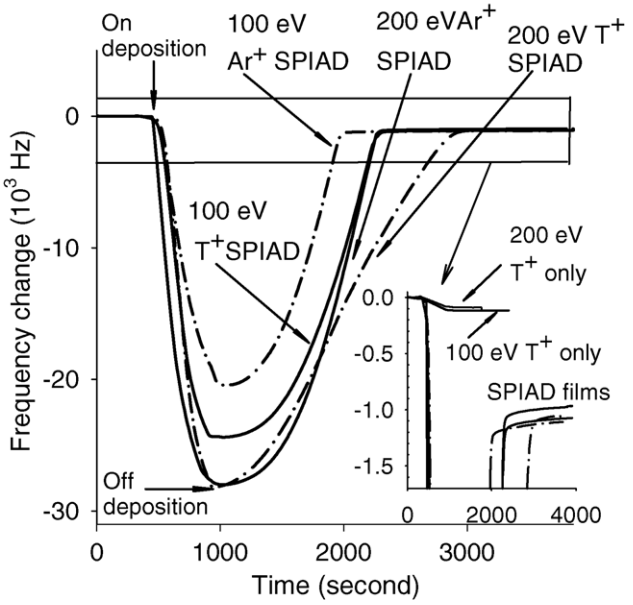

Fig. 3. Quartz crystal microbalance (QCM) frequency response during T^+ and Ar^+ SPIAD deposition at 100 and 200 eV ion energies. Inset in lower right hand corner indicates expansion of boxed region at top of graph and additionally includes QCM response for 100 and 200 eV direct thiophene ion (T^+ only) deposition.

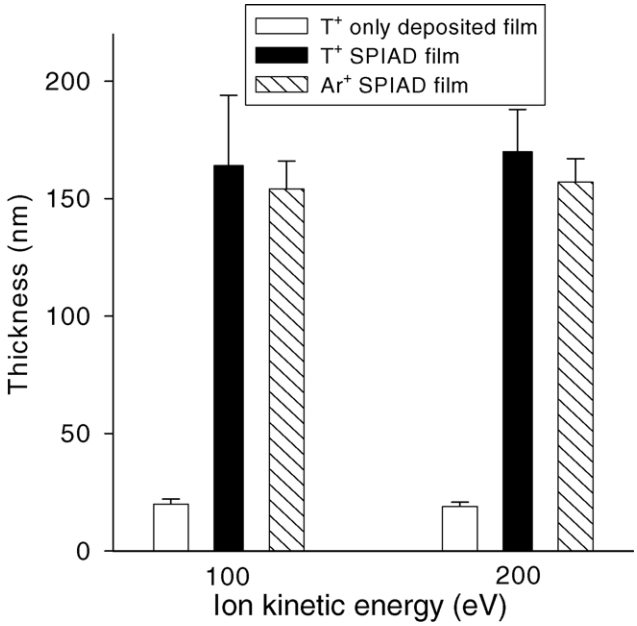

Fig. 4. QCM derived thicknesses of direct T^+ only, T^+ SPIAD, and Ar^+ SPIAD deposited films grown at 100 and 200 eV ion energies.

used. The thicknesses of 100 and 200 eV direct ion deposited films are only ~1/8 that of the SPIAD films. These results clearly confirm polymerization of 3T by SPIAD, as shown previously by other methods [9,10].

3.3. Chemical composition from mass spectra and isotopic substitution

The chemical composition of SPIAD films has been previously investigated by mass spectra of films deposited directly onto nanostructured, oxidized silicon wafers known as DIOS chips [10–12]. These results showed that several species with higher molecular weights than the original 3T neutral are present in SPIAD films, as indicated by the appearance of $[3T]T^+$, $[3T]TCH^+$, $[3T]_2{}^+$, $[3T]_2CH^+$, $[3T]_3C_3H_2{}^+$, and related ions in the mass spectra. However, it was not clear from some of these prior experiments whether the thiophene fragments which are incorporated into those ions derive from fragmented 3T or the incident thiophene ion [11,12]. Mass spectra of SPIAD films from mass-selected T^+ ions and *p*-terphenyl neutrals indicated that ions can incorporate into SPIAD films [10]. Furthermore, the role of hydrogen in the polymerization of 3T was suggested by the abundance of MH^+ peaks in the mass spectra, but the source of this hydrogen was not identified. SPIAD with Ar^+ and deuterated thiophene ions is performed here to address these issues.

Mass spectra of T^+ and Ar^+ SPIAD at 100 and 200 eV in Fig. 5 clearly show differences in the chemical species created in SPIAD films from ions of different energy and/or structure. Results for the 100 eV T^+ SPIAD films were reported previously [11] and these peak assignments are used in Table 1 for spectra of all the SPIAD film mass spectra.

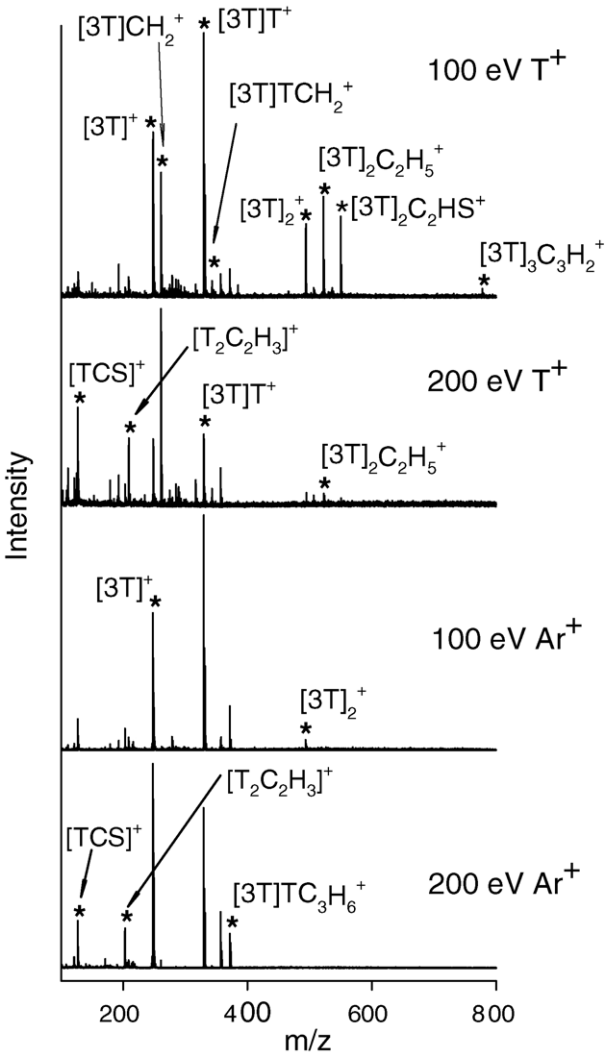

Fig. 5. Mass spectra of T^+ and Ar^+ SPIAD films grown on nanostructured silicon oxide (DIOS) substrates at 100 and 200 eV ion energies.

Table 1
Relative intensities of peaks in mass spectra of SPIAD films deposited on DIOS chips, normalized to the $[3T]^+$ peak

m/z	Ion structure	100 eV T^+	200 eV T^+	100 eV Ar^+	200 eV Ar^+
248	$[3T]^+$	1	1	1	1
261	$[3T]CH_2^+$	0.9 ± 0.3	2.1 ± 0.4	<0.01	<0.01
279	$[3T]S^+$	0.4 ± 0.2	0.3 ± 0.2	–	–
285	$[3T]C_3H_2^+$	0.1 ± 0.04	0.2 ± 0.1	–	–
317	$[3T]C_3H_2S^+$	0.2 ± 0.1	0.4 ± 0.1	–	–
330	$[3T]T^+$	1.9 ± 0.4	1.1 ± 0.3	1.6 ± 0.2	1.1 ± 0.4
342	$[3T]TCH_2^+$	0.1 ± 0.03	0.4 ± 0.1	–	–
357	$[3T]TC_2H_4^+$	0.6 ± 0.1	0.4 ± 0.1	<0.02	<0.02
372	$[3T]TC_3H_6^+$	0.4 ± 0.1	0.1 ± 0.04	0.4 ± 0.1	0.2 ± 0.1
494	$[3T]_2^+$	0.5 ± 0.1	0.3 ± 0.06	0.1 ± 0.04	–
507	$[3T]_2CH_2^+$	0.1 ± 0.02	0.2 ± 0.04	–	–
522	$[3T]_2C_2H_5^+$	0.5 ± 0.1	0.2 ± 0.1	–	–
550	$[3T]_2C_2HS^+$	0.4 ± 0.04	–	–	–
778	$[3T]_3C_3H_2^+$	<0.05	–	–	–

200 eV T^+ SPIAD films display rather different mass spectra compared to the corresponding 100 eV film: the highest molecular weight peak of the 200 eV film is $[3T]_2C_2H_5^+$ and no $[3T]_2C_2HS^+$ or $[3T]_3C_3H_2^+$ appear. The most intense peak in the 100 eV T^+ SPIAD film spectrum is $[3T]T^+$, while it is $[3T]CH_2^+$ for the 200 eV film spectrum.

Comparing further the mass spectra of the 100 eV Ar^+ SPIAD film with spectra of the corresponding 100 eV T^+ SPIAD film in Fig. 5 identifies the effect of ion structure on film chemistry. The highest molecular peak in the 100 eV Ar^+ SPIAD film spectrum is $[3T]_2^+$, whereas the highest peak in the 100 eV T^+ SPIAD film is $[3T]_3C_3H_2^+$. Furthermore, the 100 eV Ar^+ SPIAD film mass spectrum does not show any of the high molecular weight peaks corresponding to $[3T]_2CH_2^+$, $[3T]_2C_2H_5^+$, $[3T]_2C_2HS^+$, or $[3T]_3C_3H_2^+$ nor any of the lower molecular weight peaks corresponding to $[3T]CH_2^+$, $[3T]S^+$, $[3T]C_3H_2^+$, $[3T]C_3H_2S^+$, or $[3T]TCH_2^+$. Table 1 shows the relative ion intensities in the mass spectra of SPIAD films from Fig. 5 (and several additional replicate spectra, all normalized to the $[3T]^+$ peak intensity). Intensities of most of the ion peaks vary with ion structure and kinetic energy, indicating differences in the relative quantities of the corresponding species in the films. For example, the ion intensity of $[3T]CH_2^+$ in 200 eV T^+ SPIAD films is twice as high as the same ion in 100 eV T^+ SPIAD. $[3T]TC_3H_6^+$, $[3T]_2^+$, and $[3T]_2C_2H_5^+$ from the 100 eV T^+ SPIAD film all show higher intensities than from the 200 eV T^+ SPIAD film.

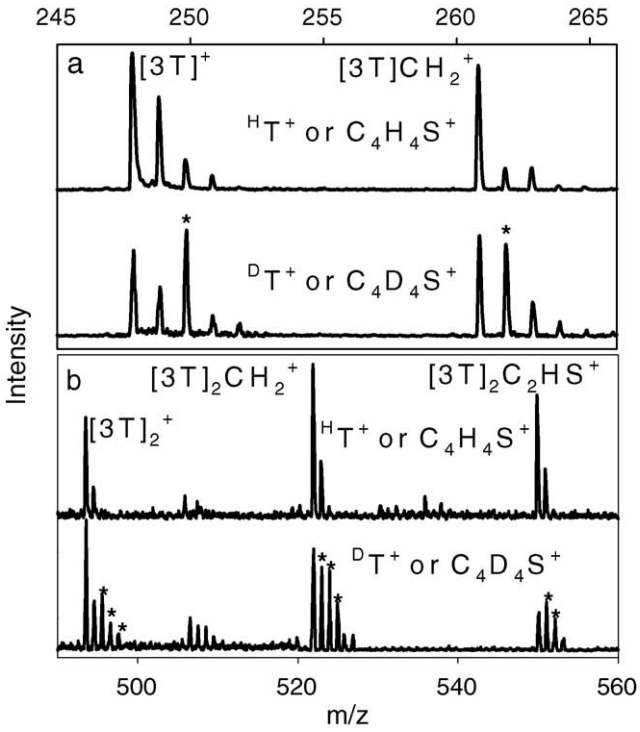

Fig. 6. Mass spectra of 100 eV SPIAD films grown on DIOS substrates from $C_4H_4S^+$ and fragments thereof (T^+) or $C_4D_4S^+$ and fragments thereof ($^DT^+$). "*" marks peaks of higher intensity for $^DT^+$ deposition.

Table 2
Relative intensities of the (M + 1) and (M + 2) peaks from mass spectra of SPIAD films prepared from 100 eV hydrogenated and deuterated thiophene ions (and fragment ions thereof), normalized to M peak intensity

m/z of M	Ion structure	M + 1		M + 2	
		$C_4D_4T^+$ or $^DT^+$	$C_4H_4T^+$ or $^HT^+$	$C_4D_4T^+$ or $^DT^+$	$C_4H_4T^+$ or $^HT^+$
248	$[3T]^+$	0.6 ± 0.1	0.6 ± 0.3	0.9 ± 0.1	0.2 ± 0.1
261	$[3T]CH_2^+$	0.9 ± 0.1	0.4 ± 0.1	0.3 ± 0.1	0.2 ± 0.05
330	$[3T]T^+$	0.6 ± 0.1	0.4 ± 0.2	0.2 ± 0.1	0.2 ± 0.05
494	$[3T]_2^+$	0.6 ± 0.1	0.4 ± 0.1	0.7 ± 0.1	0.4 ± 0.05
522	$[3T]_2C_2H_5^+$	0.8 ± 0.1	0.3 ± 0.2	0.8 ± 0.1	0.3 ± 0.1
550	$[3T]_2C_2HS^+$	0.9 ± 0.1	0.4 ± 0.1	0.8 ± 0.1	0.4 ± 0.2

Fig. 6 and Table 2 compare mass spectra of deuterated T^+ SPIAD ($^DT^+$ or $C_4D_4S^+$) films with those of hydrogenated T^+ SPIAD ($^HT^+$) films formed at 100 eV. Large differences in the intensity of the (M + 1) and/or (M + 2) peaks can be seen throughout the spectra of $^HT^+$ versus $^DT^+$, with the most notable changes indicated by "*" in Fig. 6. The (M + 2) intensity of $[3T]^+$ in $^HT^+$ versus $^DT^+$ SPIAD changes from 0.2 to 0.9, the (M + 1) intensity of $[3T]CH_2^+$ changes from 0.4 to 0.9, and the (M + 2) intensity of $[3T]_2^+$ changes from 0.4 to 0.7. Similar (M + 1) and (M + 2) intensity trends are observed for $[3T]_2C_2H_5^+$, $[3T]_2C_2HS^+$, and $[3T]_2C_2HS^+$ upon use of the deuterated ion. Other small peaks at *m/z* 279, 285, 317, 342, 357, 372, 507, and 778 cannot be compared due to large intensity fluctuations.

3.4. FTIR spectra of SPIAD films

Fig. 7 shows transmission FTIR spectra of 3T evaporated, T^+ SPIAD, and Ar^+ SPIAD films on a Si substrate

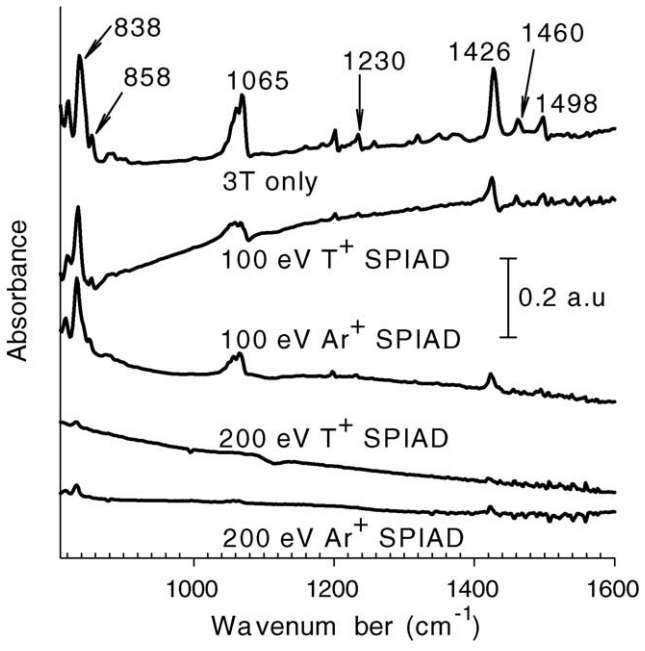

Fig. 7. Fourier transform infrared (FTIR) spectra of T^+ and Ar^+ SPIAD films grown at 100 and 200 eV ion energies on silicon substrates. Absorption unit scale indicated as "a.u."

in which the SPIAD films are scanned after 1800 s of heating with an infrared lamp and subsequent storage in vacuum for 3600 s. Peak positions of 3T evaporated films on a Si substrate are consistent with those recorded for 3T evaporated films on KBr disks: a C_α=C_β symmetric stretch appears at 1498 cm^{-1}, C_α=C_β anti-symmetric stretch at 1460 and 1426 cm^{-1}, a C_α–C_α inter-ring stretch at 1065 cm^{-1}, a C_β–H bend at 1230 cm^{-1}, and a C_α–H out-of-plane bend at 838 cm^{-1} [14,15]. The C_β–H out-of-plane bend at 798 cm^{-1} is not observed here because the Si substrate does not transmit in this spectral region. T^+ and Ar^+ SPIAD films prepared at 100 eV show strong band intensities while both 200 eV films display only very weak bands. This ion kinetic energy effect on the IR peak intensity is consistent with that on the UV–vis absorption and PL peak intensity (see above).

3.5. Crystalline structure from XRD

Evidence for crystalline structure in the 100 eV T^+ and Ar^+ SPIAD films is shown in Fig. 8, which compares their XRD with that of an 3T evaporated film. XRD of the 3T evaporated film show the strong first-, second-, and third-order reflections at 2θ angles of 6.72°, 13.63°, and 20.5°, respectively. XRD of the 100 eV Ar^+ SPIAD film displays all these 3T peaks (marked "*" when labels are adjacent to multiple peaks) and several new diffraction peaks at 19.2°, 23.20°, 25.02°, 27.98°, 28.85°, 29.53°, and 38.63°. Published XRD of sexithiophene (6T) evaporated films [16,17] allow assignment of the peaks at 19.2°, 23.20°, and 27.98° to 6T crystalline structures in the Ar^+ SPIAD films. The 28.85°, 29.53°, and 38.63° peaks in the Ar^+ SPIAD XRD remain unidentified. The 100 eV T^+ SPIAD film XRD displays two 3T peaks, but only at low intensity. The most intense peaks in the T^+ SPIAD film XRD appear at 19.33°, 19.80°, 23.20°, and 27.98°, all of which are attributed to 6T except for the unidentified 19.80° peak. The peak at 32.90° seen in the XRD of all three films is from the silicon substrate. Differences in relative 6T, 3T, and unidentified peak intensities indicate variations in the distribution of crystalline structures between the T^+ versus Ar^+ SPIAD films, with more 6T-like structures present in the former.

There are some minor differences in the spectra that depend upon post-deposition heat treatment, or the lack thereof. XRD peaks for the Ar^+ and T^+ SPIAD films only appear

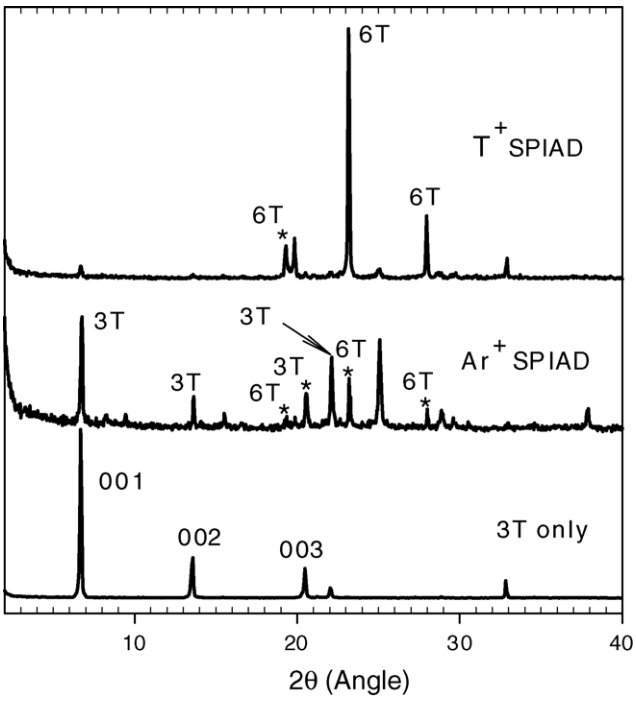

Fig. 8. X-ray diffraction (XRD) of 3T evaporated films as well as 100 eV Ar^+ and T^+ SPIAD films on silicon substrates. "*" marks peaks indicated by adjacent label.

when the films are stored in vacuum for 24 h without heating. Furthermore, all XRD peaks (except for the silicon peak) disappear as the films are heated to ~340 K for 1800 s. This indicates a loss of crystalline structure with film thickness and/or morphology. Furthermore, the relatively intense XRD peaks observed for the 100 eV SPIAD films compared with the relatively weak signals for the FTIR spectra of the same film may result in part from differences in how the films are allowed to sublime 3T. The XRD samples slowly sublime 3T over a 24 h period by storage in vacuum while the FTIR samples are forced to undergo a rapid sublimation by heating with an infrared lamp in vacuum for 1800 s. These differing treatments may change film structure in a manner not yet explored in detail. However, PL and UV–vis absorption do not depend upon these various post-deposition heat treatments, or the lack thereof (data not shown).

4. Discussion

4.1. Film growth and structure by atomic versus polyatomic ions

The various film analyses described above indicate SPIAD by both the Ar^+ atomic ion and thiophene polyatomic ions (T^+) lead to efficient polymerization compared to direct T^+ ion deposition without coincident evaporation of 3T. However, the chemical structure, crystallinity, and optical properties of the SPIAD films are all controlled by the polyatomicity and kinetic energy of the ions used to grow them.

Efficient polymerization in SPIAD is indicated by comparison of film thicknesses with those of direct ion deposited films: SPIAD films are ~160 nm thick while direct thiophene ion deposited films are only ~20 nm thick (Fig. 4). Both ions and kinetic energies yield an eightfold increase in SPIAD film growth rates compared with direct T^+ ion deposition, consistent with the tenfold increase reported previously for mass-selected ions [9,10].

The film deposition rate during SPIAD is estimated to be ~0.4 nm/s, after the sublimation of free 3T neutrals is taken into account, and is similar for polyatomic T^+ and atomic Ar^+ at either 100 or 200 eV. However, different ions and kinetic energies lead to very different film structures. Mass spectra in Fig. 5 confirm higher molecular weight species are formed by T^+ than Ar^+ SPIAD, with the different film structures explained in part by incorporation of T^+ into the film. The use of deuterated $C_4H_4S^+$ or $^DT^+$ in Fig. 6 confirms incorporation of the polyatomic ion into the film that is absent when atomic Ar^+ is used for polymerization. Furthermore, peak intensity variations for the species observed in both T^+ and Ar^+ SPIAD mass spectra indicate different distributions of the corresponding species in the films (Table 1), with higher molecular weight species favored for T^+. SPIAD film structures induced by T^+ and Ar^+ also display different crystallinity (Fig. 8). XRD of 100 eV T^+ SPIAD films display only trace 3T peaks, but prominent peaks attributed to sexithiophene (6T), consistent with the relatively high $[3T]_2^+$ observed by mass spectrometry. However, Ar^+ SPIAD films show XRD consistent with a 3T film and only minor 6T peaks, consistent with a lower intensity of $[3T]_2^+$ ions in their mass spectra (Fig. 5).

The molecular structure of the SPIAD film – composed of polymerized 3T monomer units with thiophene adducts – is destroyed by the higher ion energy, as indicated by mass (Fig. 5 and Table 1), PL (Fig. 1), and FTIR (Fig. 7) spectra. Higher mass distributions are observed in the mass spectra of 100 eV SPIAD films, regardless of the ion used. FTIR spectra of 200 eV SPIAD films display much lower vibrational band intensities compared to those of the 100 eV SPIAD films, a trend which agrees with the lower PL observed at higher ion kinetic energy. This data collectively indicate that high ion kinetic energy destroys more of the film structure upon ballistic ion impact, a phenomenon previously observed for direct polyatomic ion deposition on polymer surfaces [5,18,19].

Polymerization of 3T neutrals by SPIAD is most efficiently achieved here at a relatively low 1/100 ion to neutral ratio. This high flux of 3T for polymerization is only required because 3T neutrals sublime quickly from the substrate after deposition, as evidenced by the QCM measurement (Fig. 3). Lowering the substrate temperature to 200 K allows use of a smaller ion to neutral ratio for growth of SPIAD films from 3T (data not shown). Thus, SPIAD with higher sticking coefficients is probably likely at much larger ion to neutral ratios, which is confirmed by preliminary SPIAD work with other neutrals. Voids may also be created in the SPIAD films following sublimation of 3T. Work is underway to search for

voids which could affect overall film morphology, crystalline structure, and/or optical properties.

4.2. Polymerization mechanisms

Multiple polymerization mechanisms are found to play a role in T^+ SPIAD, where T^+ can behave as both catalyst and reagent. The catalyst or reaction initiator role is one where the kinetic energy and/or charge state of either an Ar^+ or T^+ ion induces surface polymerization of 3T. It is obvious that atomic Ar^+ can only act as a catalyst or a reaction initiator, as it cannot bond directly to 3T to form stable species. Thus, the formation of $[3T]T^+$ in Ar^+ SPIAD mass spectra (Fig. 5 and Table 1) results from Ar^+ induced fragmentation and polymerization of at least two 3T neutrals. Formation of $[3T]T^+$ and $[3T]_2{}^+$ in the mass spectra of both Ar^+ and T^+ SPIAD films can be explained by an efficient transfer of ion kinetic energy to 3T adsorbed on the surface. Previous $C_4H_4S^+$ ion scattering experiments and molecular dynamics simulations imply that the majority of the ion kinetic energy will be transferred to the 3T covered surface [20–22]. The energy of ion neutralization can also contribute to polymerization in a catalytic fashion, but this is less likely for T^+ than for Ar^+. Thiophene ion neutralization will impart at most a few eV of energy into the surface whereas Ar^+ neutralization can impart up to ∼10 eV, based upon differences in the ionization potentials of the corresponding gaseous neutrals and the surface work function.

An additional polymerization mechanism in SPIAD is where T^+ behaves as a reagent that incorporates via covalent bonding into the polymer formed. Mass-selected $C_4H_4S^+$ ions were previously found to induce polymerization of 3T and *p*-terphenyl neutrals by both the catalytic and reagent mechanisms, with the latter indicated by the incorporation of the T^+ ion into some of the polymerized p-terphenyl units [10]. A reagent role for T^+ incorporated into the SPIAD films is indicated here by the presence of 3T polymerized species with fragment ion adducts such as $[3T]_2CH_2{}^+$, $[3T]_2C_2H_5{}^+$, $[3T]_2C_2HS^+$, and $[3T]_3C_3H_2{}^+$. Such polymerized adduct species are not observed in Ar^+ SPIAD films, indicating their probable formation from $C_4H_4S^+$ fragmentation upon surface impact. For example, $[3T]_3C_3H_2{}^+$ could form from $C_3H_3{}^+$ which is a major fragment ion formed in $C_4H_4S^+$ ion-surface collisions [21,22]. Furthermore, the deuterated peaks observed in the mass spectra of $^DT^+$ SPIAD films confirms ion incorporation into the film (Fig. 6 and Table 2). Finally, about one third of the incident ions are thiophene fragment ions which significantly contribute to the polymerization event. For example, the $[3T]_2C_2HS^+$ mass spectral peak could result from incident $C_2H_2S^+$, which is a major fragment ion emitted by the non-mass-selected ion source. This argument explains why the $[3T]_2C_2HS^+$ ion is not observed in mass spectra of mass-selected T^+ SPIAD films [10].

The smallest fragment that can form either in surface collision or via direct emission from the ion source is hydrogen, either as protons or atomic hydrogen. 10 eV protons have recently been shown to induce polymerization of various adsorbed organic species by C–H bond cleavage followed by recombination of the resultant carbon radicals to form cross-linked polymeric thin films [23]. Hyperthermal protons or atomic hydrogen also play a role in SPIAD. An abnormally high intensity of protonated (M + 1) peaks in SPIAD film mass spectra was observed previously and attributed to free hydrogen atoms or protons in the film [11]. However, this previous work did not determine whether the source of this extra hydrogen was surface induced dissociation of incident T^+ or adsorbed 3T. If hydrogen from neutrals contributes to polymerization, then some high molecular weight peaks containing extra hydrogen (M + 1) observed in the 100 eV T^+ SPIAD film should also appear in the Ar^+ SPIAD film spectra. However, 100 eV Ar^+ SPIAD does not show such (M + 1) peaks, indicating that the incident T^+ ion is the source of most extra hydrogen. Significant contribution to polymerization by protons from incident T^+ ion is confirmed by the appearance of deuterated ions in the mass spectra of films grown from $^DT^+$ (Fig. 6).

The similar enhancements for mass-selected versus non-mass-selected ion SPIAD discussed above indicate that non-ion-assisted mechanisms are not the predominant contributor to film polymerization in these SPIAD experiments. Nevertheless, there is probably some enhancement in polymerization of 3T neutrals by radicals, photons, or electrons emitted from the broad beam ion source. Thermal excitation and/or ultraviolet irradiation from a hot filament can initiate polymerization [24–26]. Furthermore, 3T neutrals on nanostructured titanium oxide surfaces can be photopolymerized to 6T by UV irradiation [27]. Hot filament or photopolymerization of 3T neutrals is possible here, but it is unknown if the optical emission from the broad beam ion source is of sufficient intensity and appropriate wavelength to induce photopolymerization. Another inadvertent event here could be electron induced polymerization, which was observed previously for 3-hexylthiophene monomer on surfaces [28,29]. However, no difference is observed in optical properties and mass spectra for 200 eV T^+ SPIAD films grown with and without a voltage biased substrate. The substrate biasing modulates the electron flux and confirms electron induced polymerization is not a dominant effect here. Overall, while non-ionic particles emitted from the ion source may contribute to polymerization during SPIAD, these effects appear minor. This point is especially clear when the data are compared with mass-selected ion experiments (where such non-ionic particles are absent) which give many similarities in polymerization and unequivocally show that a pure ion-induced polymerization is also occurring here [10].

4.3. Control of optical properties

It was previously reported that ion energy controls optical properties of SPIAD films, leading to red shifts in the PL and film band gaps compared to the 3T evaporated films

[11]. The shift in optical properties was attributed in part to an increase in conjugation length of the molecular constituents of the SPIAD films, a result consistent with the observed optical properties of 3T photopolymerized to 6T [27]. The different optical properties of SPIAD films by polyatomic T^+ and atomic Ar^+ observed in the present work can also be explained by differences in polymerization induced by these two ions. As higher molecular weight peaks are observed in mass spectra of the T^+ SPIAD film, the UV–vis absorption peak shifts to the red. This red shift is greater for the T^+ SPIAD film than for the Ar^+ SPIAD film, consistent with the higher molecular weight species in the former.

In addition to the aforementioned effect of higher molecular weight species on the optical properties of SPIAD films formed by different ion structures, previously observed blue shifts in PL of some of these films indicated an additional role for aggregation effects [11]. Film aggregation of SPIAD films may be correlated with high content of protons due to their likely ability to cross-link these films. Many reports have demonstrated that differing aggregation in conjugated oligomer or polymer films can cause significant changes in optical properties including shifts in PL and UV–vis absorption [17,30]. Aggregation effects are also clearly related to film crystalline structure, which in turn contributes to optical properties [16]. It follows that the different crystalline structures of Ar^+ and T^+ SPIAD films also contribute here to the different optical properties.

5. Conclusion

It is found that both non-mass-selected hyperthermal T^+ and argon ions induce polymerization of 3T neutrals on surfaces at hyperthermal kinetic energies. While atomic Ar^+ ions behave only as catalysts of polymerization during SPIAD, $C_4H_4S^+$ polyatomic ions and their fragments additionally behave as reagents which covalently bind to 3T. Protons or atomic hydrogen produced mostly from fragmentation of the incident T^+ ion also induce polymerization, as has been recently observed through direct deposition of 10 eV protons on organic films [23]. Polyatomic and atomic ions lead to significantly different film chemistry and optical properties, which also vary for 100 versus 200 eV ion kinetic energies. Overall, 100 eV T^+ SPIAD produces films with the highest molecular weight species of the films examined here. These results show that SPIAD films produced by polyatomic ions are in fact distinct from those produced by atomic ion-assisted deposition [4,6], indicating a role of the polyatomicity of the incident ion. The use of distinct ion and neutral sources therefore appears justified in SPIAD, in contrast to other methods that incorporate one source for both species [7,8]. Variation of the polyatomic ion structure will lead to production of a yet wider range of conducting polymers. This is especially clear when considered in conjunction with recent work that has shown the modification of band gaps and other useful electronic properties of SPIAD conducting polymer films ([11] and work to be published).

Acknowledgements

This work is funded by the National Science Foundation (NSF) under Award No. CHE-0241425. The authors thank Professor Steve Guggenheim for training on and use of his X-ray diffraction instrument. Finally, LH would like to thank Bill Hase for his mentoring and past collaborations. His work is impeccable, his assistance unstinting, and his example to scientists everywhere without peer. Bill has been and continues to be everything a fine scientist should be.

References

[1] A.J. Heeger, J. Phys. Chem. B 105 (2001) 8475.
[2] D. Fichou (Ed.), Handbook of Oligo- and Poly-thiophenes, Wiley-VCH, Weinheim, 1999.
[3] M. Leclerc, K. Faid, Adv. Mater. 9 (1997) 187.
[4] A. Moliton, in: T.A., Skotheim, R.L., Elsenbaumer, J.R., Reynolds (Eds.), Handbook of Conducting Polymers, New York, 1998, p. 589.
[5] L. Hanley, S.B. Sinnott, Surf. Sci. 500 (2002) 500.
[6] R. Antony, A. Moliton, B. Ratier, Appl. Phys. B 71 (2000) 33.
[7] H. Usui, Thin Solid Films 365 (2000) 22.
[8] J.-Y. Kim, E.-S. Kim, J.-H. Choi, J. Appl. Phys. 91 (2002) 1944.
[9] S. Tepavcevic, Y. Choi, L. Hanley, J. Am. Chem. Soc. 125 (2003) 2396.
[10] S. Tepavcevic, Y. Choi, L. Hanley, Language 20 (2004) 8754.
[11] Y. Choi, S. Tepavcevic, Z. Xu, L. Hanley, Chem. Mater. 16 (2004) 1924.
[12] L. Hanley, Y. Choi, S. Tepavcevic, Mater. Res. Soc. Symp. Proc. 804 (2004) JJ5.3.1.
[13] J. Wei, J.M. Buriak, G. Siuzdak, Nature 399 (1999) 243.
[14] Y. Furukawa, M. Akimoto, I. Harada, Synth. Metals 18 (1987) 151.
[15] G. Louarn, J.P. Buisson, S. Lefrant, D. Fichou, J. Phys. Chem. 99 (1995) 11399.
[16] B. Servet, et al., Chem. Mater. 6 (1994) 1809.
[17] G. Horowitz, B. Bachet, A. Yassar, P. Lang, F. Demanze, J. Fave, F. Garnier, Chem. Mater. 7 (1995) 1337.
[18] M.B.J. Wijesundara, Y. Ji, B. Ni, S.B. Sinnott, L. Hanley, J. Appl. Phys. 88 (2000) 5004.
[19] F.A. Akin, et al., J. Phys. Chem. B 108 (2004) 9656.
[20] L. Hanley, H. Lim, D.G. Schultz, S.B. Wainhaus, P.d.S. Claire, W.L. Hase, Nucl. Instrum. Meth. Phys. Res. B 125 (1997) 218.
[21] H. Lim, D.G. Schultz, E.A. Gislason, L. Hanley, J. Phys. Chem. B 102 (1998) 4573.
[22] H. Lim, D.G. Schultz, E.A. Gislason, L. Hanley, J. Phys. Chem. B 102 (1998) 9362.
[23] Z. Zheng, X. Xu, X. Fan, W.M. Lau, R.W.M. Kwok, J. Am. Chem. Soc. 126 (2004) 12336.
[24] M. Tamada, H. Omichi, N. Okui, Thin Solid Films 251 (1994) 36.
[25] M.C. Kwan, K.K. Gleason, Chem. Vap. Deposition 3 (1997) 299.
[26] M. Tamada, H. Koshikawa, F. Hosoi, T. Suwa, H. Usui, A. Kosaka, H. Sato, Polymer 40 (1999) 3061.
[27] C.L. Huisman, A. Huijser, H. Donker, J. Schoonman, A. Goossens, Macromolecules 37 (2004) 5557.
[28] J.E. Hernandez, H. Ahn, J.E. Whitten, J. Phys. Chem. B 105 (2001) 8339.
[29] H. Ahn, J.E. Whitten, J. Phys. Chem. B 106 (2002) 11404.
[30] B.J. Schwartz, Annu. Rev. Phys. Chem. 54 (2003) 141.